energies

MDPI

Article

Comparison of Cycle Reduction and Model Reduction Strategies for the Design Optimization of Hybrid Powertrains on Driving Cycles

Adham Kaloun [1,2,*], Stéphane Brisset [1], Maxime Ogier [3], Mariam Ahmed [2] and Robin Vincent [2]

[1] Arts et Metiers Institute of Technology, Université de Lille, Centrale Lille, Junia, ULR 2697-L2EP, F-59000 Lille, France; stephane.brisset@centralelille.fr
[2] Valeo Equipements Electrique Moteur, 94400 Créteil, France; mariam.ahmed@valeo.com (M.A.); robin.vincent@valeo.com (R.V.)
[3] CNRS, Université de Lille, Inria, Centrale Lille, UMR 9189 CRIStAL, F-59000 Lille, France; maxime.ogier@centralelille.fr
* Correspondence: adham.kaloun@phd.centralelille.fr

Abstract: Decision-making is a crucial and difficult step in the design process of complex systems such as the hybrid powertrain. Finding an optimal solution requires the system feedback. This can be, depending on the granularity of the models at the component level, highly time-consuming. This is even more true when the system's performance is determined by its control. In fact, various possibilities can be selected to deliver the required torque to the wheels during a driving cycle. In this work, two different design strategies are proposed to minimize the fuel consumption and the cost of the hybrid powertrain. Both strategies adopt the iterative framework which allows for the separation of the powertrain design problem and its control while leading to system optimality. The first approach is based on model reduction, while the second approach relies on improved cycle reduction techniques. They are then applied to a parallel hybrid vehicle case study, leading to important cost reduction in reasonable delays and are compared using different metrics.

Keywords: cycle reduction; hybrid electric vehicle; model reduction; optimal control; optimal design; electric machines; Plant/Controller optimization

Citation: Kaloun, A.; Brisset, S.; Ogier, M.; Ahmed, M.; Vincent, R. Comparison of Cycle Reduction and Model Reduction Strategies for the Design Optimization of Hybrid Powertrains on Driving Cycles. *Energies* **2021**, *14*, 948. https://doi.org/10.3390/en14040948

Academic Editor: Roberto Finesso

Received: 10 December 2020
Accepted: 2 February 2021
Published: 11 February 2021

1. Introduction

An increasing number of car makers are turning towards hybridization technologies to meet stricter environmental regulations [1,2]. To exploit this concept further, improving the overall efficiency of the hybrid powertrain is paramount. However, it has been shown that there is a strong coupling between the design and control problems, even between powertrains of similar performances (peak power, torque, and speed) [3]. This impacts the design process by adding thousands of optimization variables for typical conception cycles.

Different frameworks are used to solve plant/controller optimization problems, to which hybrid powertrain optimization belongs: sequentially, iteratively, using a bi-level approach or simultaneously [4]. The sequential approach is where the design is optimized first for a certain control strategy, before optimizing the command afterwards. The iterative approach improves the solution of the sequential method by re-optimizing the design following significant changes in the controller's command, before reiterating again until convergence. Meanwhile, the bi-level approach finds the optimal control for each design proposed by a top level algorithm. Finally, the simultaneous approach solves the global optimization problem directly by finding the optimal values for control and design variables simultaneously.

The sequential method does not guarantee a system optimum [5]. The remaining frameworks however can guarantee system optimality as they consider the coupling between design and control optimizations and have been extensively addressed for hybrid

powertrain optimization: the authors of [6–13] implemented the bi-level framework using dynamic programming to optimize power management and explored different mono-objective and multi-objective optimization algorithms for the design problem (Sequential Quadratic Programming, genetic algorithms, Particle Swarm Optimization, and DIviding RECtangles). Although robust, this approach is very time-consuming as it optimizes the control strategy at every iteration. Thus, it leads to additional challenges when using heavy models and trying to find an optimal solution in reasonable delays. The simultaneous approach, which considers all of the variables at once, requires a much higher number of resources to be allocated and has limited applications [14,15] finds non-convergence problems when using the simultaneous approach for a large number of decision variables. This forces him to only use it for short driving cycles. The authors of [16,17] managed to apply it by adjusting the design parameters and the parameters of a simplified rule-based strategy to select the best power split between the engine and the electric machine of a parallel powertrain using genetic algorithms. This reduces the complexity of command optimization and leads to a lower number of decision variables to be optimized, which then enables faster convergence of the optimization algorithm. However, application of these approaches requires very high computation times. The authors of [18] relied on the iterative scheme to develop an analytical target cascading approach, which starts from the system specifications to deduce the components requirements, and applied it for fast optimization of a power-split hybrid powertrain. This method is however better suited when there is a need to optimize multiple physical components with strong interactions [19]. Other promising possibilities offered by the iterative framework still need to be thoroughly investigated as well.

In this paper, two new hybrid powertrain optimization methods, based on the iterative framework, are presented and compared. They are used primarily to optimally design the electric machine (EM) of a parallel hybrid powertrain over driving cycle while considering system interactions.

The first proposed variant uses an EM losses mapping model to assess the machine's performance over the driving cycle. This model is calculated using a limited number of finite elements (FE) simulations in order to approximate the evolution of the captured flux and iron losses with the imposed current. These response surfaces are implemented in an equivalent electric circuit model which is much faster to evaluate.

The second alternative relies on cycle reduction techniques to drastically reduce the number of operating points, focusing only on a limited pool of interest points. This can allow the direct use of heavy model simulations to accurately determine the losses of the EM and evaluate the fuel consumption without leading to long computation times. Different cycle reduction methods are analyzed and studied. These methods are improved with new techniques such as mirroring to minimize the number of required operating points needed to achieve a specific precision.

The remainder of the paper presents the hybrid electric vehicle (HEV) case study as well as the models used for the various powertrain elements. Special emphasis is given to the electric machine, as different models of varying granularity are exploited to consider the impact of the design parameters on performance. The coupled optimization problem is defined afterwards before highlighting how the proposed approaches are applied. Finally, the results of the systemic design applications and conclusions are presented.

2. Hybrid Vehicle Case Study

In this paper, a compact vehicle equipped with a parallel hybrid powertrain is considered. This means it incorporates an internal combustion engine (ICE) and an EM, both of which can provide, either simultaneously or separately, the required torque to the wheels, as seen in Figure 1. The electric machine's shaft is connected to the transmission via a fixed ratio gear set. A clutch allows the ICE to disconnect from the rest of the powertrain, reducing the braking torque. The EM, on the other hand, is always connected to the transmission shaft and is powered by a lithium battery.

The powertrain provides the required mechanical energy to negate the driving resistances applied to the vehicle when it is moving: the vehicle's weight, the rolling resistance, and the aerodynamic drag. These forces are calculated using analytic expressions [20] and based on the vehicle's characteristics, speed, and road conditions.

In this work, indoor settings are considered where the vehicle is on flat roller benches connected to air blowing systems. The backward approach is adopted afterwards, where the target speed is always achieved.

The vehicle model's outputs are evaluated using a discretized time range and quasi-static models of the powertrain components. The powertrain model also assumes isothermal conditions of the components. This means the impact of temperature and other dynamic phenomena on the performance of the components is neglected.

A fuel consumption and electric losses mappings which depend on torque and rotation speed are used for the engine and EM block respectively. The latter includes the machine and inverter. These models are more accurate than efficiency mappings, especially during takeoff and low values of delivered torque.

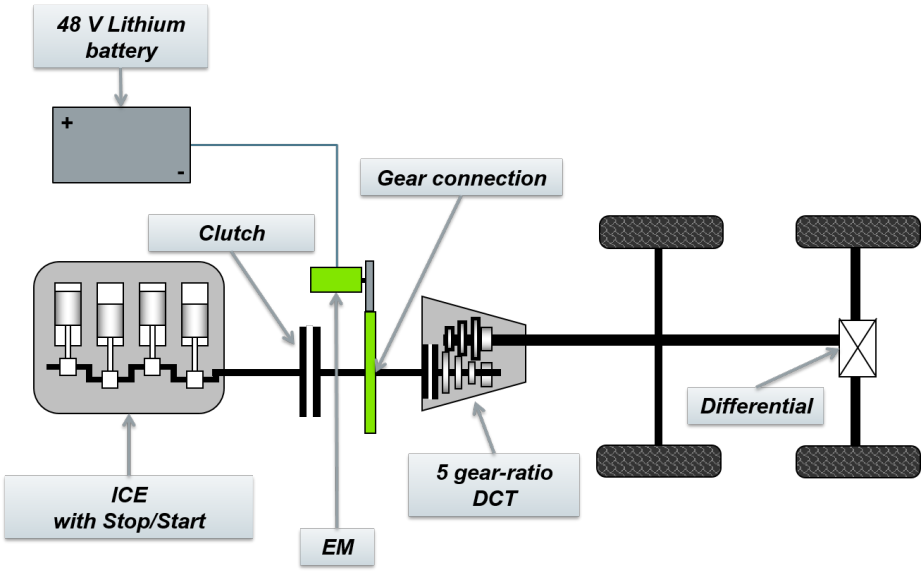

Figure 1. Studied powertrain.

The ICE's inertia is used to calculate the starter's electrical energy consumption during the ICE's restart, as the engine can be turned off to cut pumping losses and reduce fuel waste. At low speed, the ICE runs at specific idle speed to operate reasonably smoothly.

The battery uses a simplified circuit model made of an internal resistance connected in series with an open circuit voltage, whose values are assumed independent of the state of charge value. Its usage is restricted between 30% and 70% of its total charge, to limit premature aging. The battery powers both the electric machine and engine starter, as well as the 12 V auxiliary network using a DC/DC converter.

The transmission model relies on an efficiency mapping which depends on the transmission speed, mechanical torque provided and the selected gear. Energy loss during gear shifting has also been considered. Only one upshift or downshift is possible at each time step to respect the gearbox's mechanical constraints. The vehicle model is detailed further in [3].

3. Electric Machine Block

The electric machine is at the core of the optimization application. Thus, more emphasis is given to this component and how its design parameters impact its performance and losses. This section presents the design variables $\boldsymbol{d}$ considered before explaining how the different inputs and models are integrated to form the EM block.

3.1. Permanent Magnet Synchronous Machine Parametric Model

For this paper, the machine is a V-shape inserted permanent magnet synchronous machine (VI-PMSM). Twenty-seven machine parameters are then defined to enable a high degree of design flexibility. The number of pole pairs p and the number of slots per pole N_{slot} can be modified as well as other geometrical design parameters shown in Figure 2.

The selected model uses distributed winding and considers 4 additional winding parameters that can be adjusted: the number of series and parallel conductors, referred to as N_{series} and N_{parallel}, respectively; the nature of the winding connection Wnd_{Con}; and the number of winding phases N_{ph}. The materials used for the different machine parts are imposed. Copper is adopted as a winding conductor, while steel sheets are applied for the stator and rotor cores, and high-performance NdFeB magnets are used to generate the rotor field.

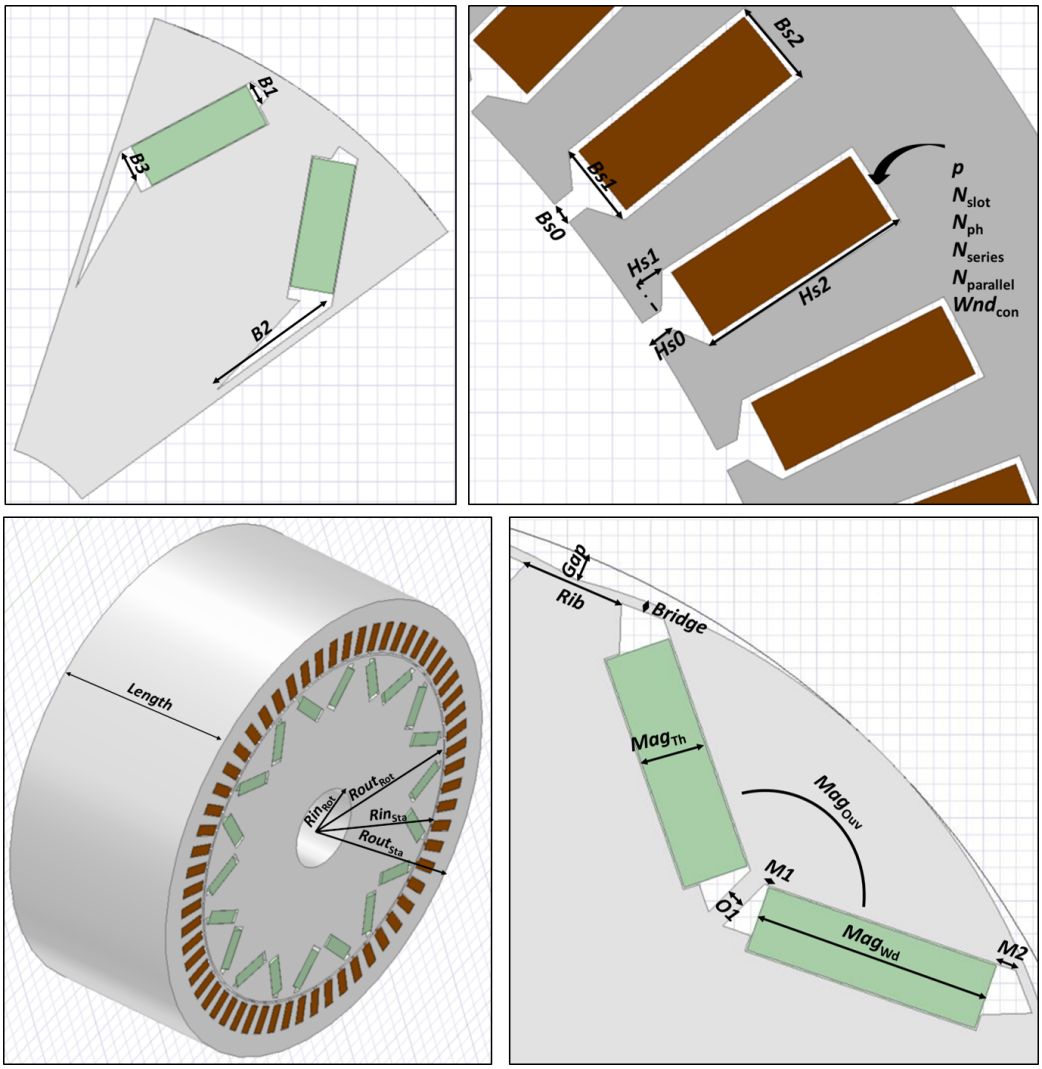

Figure 2. Machine design parameters.

In this work, two switching strategies can be used by the inverter to convert the DC power supply to an AC power supply: Pulse Width Modulation (PWM) and Full Wave (FW). The PWM strategy is selected for less output harmonic content while the FW strategy allows for less switching losses and higher current magnitudes. $Speed_{\text{FWM}}$, referring to the machine's rotational speed in rpm as of which the inverter switches from a PWM to a FW strategy, is considered as an additional design variable as well as R_{GC}, the ratio of the torque coupler.

3.2. EM Losses

In order to evaluate the mechanical torque of the machine for a certain electrical power input, the machine losses $Losses_{\mathrm{EM}}$ need to be defined. In this study, they are expressed as

$$Losses_{\mathrm{EM}} = Losses_{\mathrm{Mech}} + Losses_{\mathrm{Joule}} + Losses_{\mathrm{Iron}} + Losses_{\mathrm{Inverter}} \quad (1)$$

with $Losses_{\mathrm{Mech}}$, $Losses_{\mathrm{Joule}}$, $Losses_{\mathrm{Iron}}$, and $Losses_{\mathrm{Inverter}}$ referring to the mechanical, Joule, iron, and inverter losses, respectively, in W. These losses depend on the machine's design parameters $\boldsymbol{d}$ and its operation point defined by the injected current amplitude I in A, the current angle ϕ in rad and the machine's rotational speed ω_{EM} in rpm.

Analytic models are used to express the mechanical losses, Joule losses, which include DC and AC losses, and inverter losses. As iron losses require the knowledge of the magnetic flux density distribution in the iron core of the designed machine [21], a Finite Element (FE) model is used to guarantee precise results. This model should also allow for the precise calculation of the machine's output torque T_{EM}.

3.3. Finite Element Model

A parametric FE model is established afterwards. In the case of an on-load analysis, the machine geometry, electrical circuit properties, as well as the rest of the study parameters are defined using the previously introduced parametric model and based on the values of $\boldsymbol{d}$, I, ϕ, and ω_{EM}. Once the FE calculations have converged, the requested quantities are available as outputs of the model. The described model will also be used for no-load and short circuit scenarios, providing the short-circuit current in the latter case for example.

The parametric FE model's results are then compared to those of the experimental bench test results. Acceptable deviations of less than 2% have been found, as detailed in Appendix A. However, besides a desirable level of precision, the model implemented to determine the machine's performance should require reasonably short calculation times. Even with various adjustments to accelerate computation, such as simulation of only the 2D pole section, it still requires about one minute to evaluate the machine's performance over a single operation point (comparison on the same work station equipped with an i7-6820HQ processor at 2.7 GHz and 31.8 GB of RAM, and using the Windows 10 Pro operating system). Thus, other possibilities should be explored to develop a more suitable model that can be used for the optimization study.

3.4. Circuit Model

The PMSM operation at different rotational speeds can be assessed using Park's representation [22]. Through this transformation, the different AC wave forms are simplified into DC signals. Furthermore, when studying a balanced three-phase system, the equivalent circuit model can be used to describe the machine.

For a fixed machine design, the direct and quadrature flux linkage component values ψ_{d} and ψ_{q} are assumed dependent only on the values of injected current components i_{d} and i_{q}. Analytic expressions for machine losses are applied afterwards and the different components of the iron losses are expressed as

$$Losses_{\mathrm{Iron}} = k_{\mathrm{Hys}}(i_{\mathrm{d}}, i_{\mathrm{q}})\omega_{\mathrm{EM}} + k_{\mathrm{EC}}(i_{\mathrm{d}}, i_{\mathrm{q}})\omega_{\mathrm{EM}}{}^2 \quad (2)$$

where k_{Hys} and k_{EC} are the hysteresis losses coefficient in W.s/rad and the eddy current losses coefficient in W.s^2/rad^2, respectively, and are supposed to vary, similarly to the flux linkage components, only with respect to both the direct and quadrature values of the injected currents and ω_{EM} the EM's rotational speed in rpm.

Response surfaces are used for the loss coefficients and flux linkage models, based on the simulation results of the parametric FE model launched at a selected rotation speed for different values of (i_{d}, i_{q}). Based on the stated assumptions, these values can be used as well for other revolution speeds. If more values for i_{d} and i_{q} are considered when establishing

the response surfaces, the accuracy of the circuit model will be improved. However, the required time increases even if parallel computing has helped accelerate this process.

The number of required values to select for (i_d,i_q) to achieve acceptable accuracy and complete the circuit model depends on the value of the maximum current output I_{max} and the machine geometry. Afterwards, the model will allow for the quick assessment of $Losses_{EM}$, the phase-neutral voltage amplitude V, and the output torque T_{EM} for different values of (I, ϕ, ω_{EM}).

3.5. Losses Mapping Model

Once the circuit model is established for a set of design variables $\boldsymbol{d}$, a losses mapping model is calculated: first of all, the rotation speed range of the EM is discretized into discrete values ω_i. Afterwards, the maximum torque provided by the machine in motor mode $\boldsymbol{T_{EM,max}}$ in N.m is calculated for each value of ω_i as follows,

$$T_{EM,max}(\boldsymbol{d}, \omega_i) = \max_{\phi} \; T_{EM}(I_{max}, \phi, \boldsymbol{d}, \omega_i) \tag{3a}$$

$$\text{subject to} \quad V(I_{max}, \phi, \boldsymbol{d}, \omega_i) \leq V_{max}(\boldsymbol{d}) \tag{3b}$$

$$\phi \in [\frac{\Pi}{2}, \Pi] \tag{3c}$$

where V_{max} is the maximum voltage threshold which depends on the power supply, winding configuration, and inverter switching strategy. The different values for the torque and voltage are expressed using the circuit model. The minimum torque values of the machine $\boldsymbol{T_{EM,min}}$ in generator mode in N.m are also calculated by solving the following optimization problem for

$$T_{EM,min}(\boldsymbol{d}, \omega_i) = \min_{\phi} \; T_{EM}(I_{max}, \phi, \boldsymbol{d}, \omega_i) \tag{4a}$$

$$\text{subject to} \quad V(I_{max}, \phi, \boldsymbol{d}, \omega_i) \leq V_{max}(\boldsymbol{d}) \tag{4b}$$

$$\phi \in [\Pi, \frac{3\Pi}{2}] \tag{4c}$$

As a result, the envelope of the operation region is defined, as shown in Figure 3 and the machine's mechanical torque range is known. The latter is discretized into discrete values T_j for each value of ω_i. The optimal machine control for different values of (ω_i,T_j) inside the machine operation range needs to be calculated afterwards. This is defined as values for the current supply that minimize the machine's losses at each operation point, which is expressed as

$$\min_{I,\phi} \quad Losses_{EM}(I, \phi, \omega_i, \boldsymbol{d}) \tag{5a}$$

$$\text{subject to} \quad V(I, \phi, \omega_i, \boldsymbol{d}) \leq V_{max}(\boldsymbol{d}) \tag{5b}$$

$$T_{EM}(I, \phi, \omega_i, \boldsymbol{d}) = T_j \tag{5c}$$

$$I \in [0, I_{max}] \tag{5d}$$

$$\phi \in [\frac{\Pi}{2}, \frac{3\Pi}{2}] \tag{5e}$$

The losses mapping of the selected machine, delimited by its envelope is then defined, as seen in Figure 4. The EM's electrical power consumption P_E for a selected operation point is then deduced as well. For imposed values of ω_{EM} and $\boldsymbol{d}$, P_E is a bijective function of T_{EM}, as it is strictly monotonous with respect to the latter. As a result, T_{EM} can be deduced for any set of values of (ω_{EM},$\boldsymbol{d}$, P_E), and thus any set of values (ω_{EM},$\boldsymbol{d}$, I).

Therefore, this model allows for the quick and direct assessment of the machine's optimal losses at any operation point defined by T_{EM} and ω_{EM} without the additional time required to determine the optimal command, and is used for both the hybrid powertrain's power management and calculation of its fuel consumption.

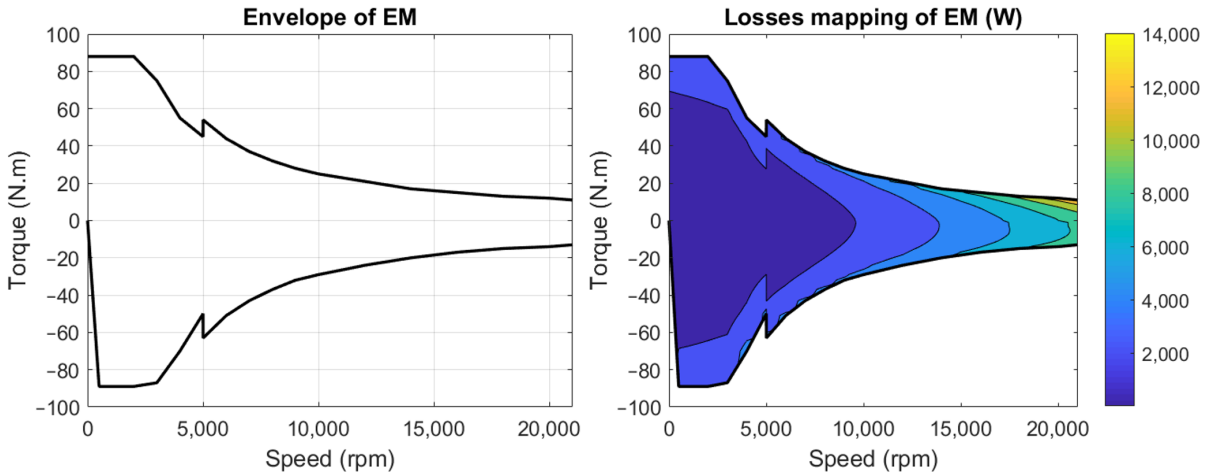

Figure 3. Left: Example of EM operation envelope. **Right**: Example of EM losses mapping. The maximum torque region can be identified, as well as the maximum power region. The torque peak in the maximum power region corresponds to a change in the inverter's switching strategy ($Speed_{\mathrm{FWM}}$ = 5000 rpm).

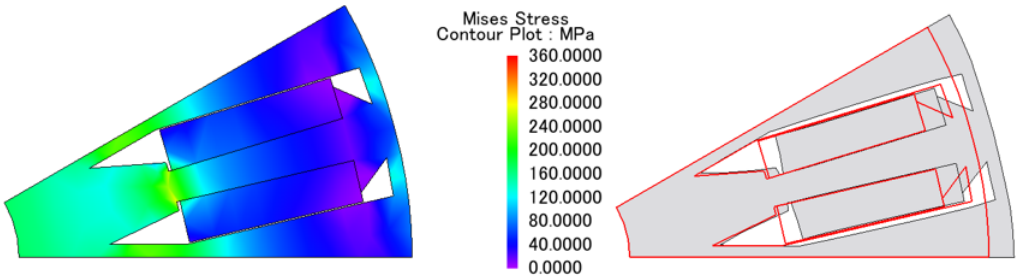

Figure 4. Mechanical simulation of rotor core at overspeed in JMAG. **Left**: Levels of Stress. **Right**: Deformation of rotor amplified at 100 times.

4. Optimization Problem

4.1. Problem Formulation

Different objectives can be studied when optimizing the hybrid powertrain such as the minimization of various types of emissions, improving the vehicle's fuel economy over a specific driving cycle, or reducing the powertrain's total cost.

In this work, both of the latter objectives are considered and the hybrid powertrain optimization problem is formulated as

$$\underset{\boldsymbol{d},\boldsymbol{u}}{\text{minimize}} \quad J(\boldsymbol{d},\boldsymbol{u}) = \alpha Inv(\boldsymbol{d}) + \beta \sum_{t_0}^{t_f-\Delta t} L(\boldsymbol{d},\boldsymbol{x}(t),\boldsymbol{u}(t),t)\Delta t \tag{6a}$$

$$\text{subject to} \quad \boldsymbol{x}(t+\Delta t) = \boldsymbol{f}(\boldsymbol{x}(t),\boldsymbol{u}(t),t)\Delta t + \boldsymbol{x}(t) \tag{6b}$$

$$x_1(t_0) = x_0 \tag{6c}$$

$$x_1(t_f) = x_f \tag{6d}$$

$$\boldsymbol{g}(\boldsymbol{d},\boldsymbol{x}(t),\boldsymbol{u}(t),t) \leq 0 \tag{6e}$$

$$\boldsymbol{k}(\boldsymbol{d}) \leq 0 \tag{6f}$$

$$\boldsymbol{x}(t) \in [\boldsymbol{x}_{\mathbf{min}}(t), \boldsymbol{x}_{\mathbf{max}}(t)] \tag{6g}$$

$$\boldsymbol{u}(t) \in [\boldsymbol{u}_{\mathbf{min}}(t), \boldsymbol{u}_{\mathbf{max}}(t)] \tag{6h}$$

$$\boldsymbol{d} \in [\boldsymbol{d}_{\mathbf{min}}, \boldsymbol{d}_{\mathbf{max}}] \tag{6i}$$

where L is the instantaneous fuel consumption in g/s which is calculated using the system model described in Section 2 and Inv is the powertrain cost in €. As the EM is the only powertrain component being modified while the rest of the drivetrain remains unchanged

during the optimization process, only the cost of the EM matters and is considered in this work as a function of its peak power. The following expression is proposed [23–25]:

$$Inv(\boldsymbol{d}) = 1000 + 0.02P_{\max}(\boldsymbol{d}) \tag{7}$$

This proposition is valid for the selected machine topology and application power range, as well as the fact that the active part materials are imposed. Detailed functions separating the material and manufacturing costs could have been applied here as well. The values for α and β are selected to bring both terms of the cost function together. For this work, α is equal to 1 and the following expression is proposed for β, which considers the penalty payment for CO_2 emissions target exceedance:

$$\beta = \frac{Pen\ Conv_{\text{lgasoline-gCO}_2}}{\rho_{\text{gasoline}}\ Dist_{\text{cycle}}} \tag{8}$$

where *Pen* is the emissions target exceedance penalty value, equal to 95 € /(gCO_2/km) in Europe since 2019, while $Conv_{\text{lgasoline-gCO}_2}$ converts liters of gasoline consumption into grams of CO_2 emissions. ρ_{gasoline} is the gasoline's density in g/l and $Dist_{\text{cycle}}$ is the selected driving cycle's distance in km.

$\boldsymbol{x}$ refers to the state variables and has three components: the state of charge of the battery *SoC*, the selected gear, and the state of the engine. $\boldsymbol{u}$ represents the command variables and is directly linked to the variations of $\boldsymbol{x}$ and as a result also has three components (u_1: $\Delta SoC(t)/\Delta$t; u_2: gear switch; u_3: starter command). Thus, the evolution function $\boldsymbol{f}$ only depends on the command variables and corresponds to the identity function, while considering the discrete/continuous nature of each variable.

The charge sustaining condition, also called iso-SoC condition, is considered in this application as well and is expressed in Equation (9) regarding the imposed initial and final value of the state of charge x_0 and x_f, respectively. It is an important criterion for HEV homologation, as it imposes that the energy used during the driving cycle only comes from the fuel tank. This in turn means that the energy stored in the battery at t_0 should be found by the end of the driving cycle at t_f.

$$x_0 = x_f \tag{9}$$

$\boldsymbol{g}$ refers to the command inequality constraints function, while $\boldsymbol{k}$ represents the design inequality constraints that need to be satisfied by the proposed optimal solution. Both optimization constraints are detailed afterwards. The various optimization variables are also limited by their respective lower and upper bounds.

4.2. Command Constraints

The command constraints are linked to powertrain component limitations. In this work, the values for the different command variables will need to consider the maximum and minimum output torque of the EM and maximum output torque of the ICE, as well both their maximum rotational speeds.

4.3. Design Constraints

Aside from command constraints, design constraints need to be considered as well when optimizing the hybrid powertrain. The design constraints are related to the electric machine, as it is the sole component whose design is modified in this application. These are deduced by analyzing the machine specifications while considering machine design standards and restrictions to guarantee a coherent design. The different design considerations are detailed afterwards and are classified into

- geometric constraints,
- performance constraints,
- process constraints,
- mechanical constraints,
- thermal constraints,

- demagnetization constraints,
- torque ripple constraints, and
- inverter constraints.

4.3.1. Geometric Constraints

The geometric constraints need to be verified for each machine design and will ensure the machine's mechanical integrity and the ability of the parametric model to provide a consistent machine geometry. These constraints are expressed in the form of analytical inequalities that need to be satisfied in order to have a valid design.

It is also worth mentioning that the air gap value is fixed afterwards. Thus, only the rotor's external radius $Rout_{\mathrm{Rot}}$ is considered, while the value of the stator's internal radius Rin_{Sta} is deduced from the latter.

4.3.2. Performance Constraints

The performance constraints are related to the peak torque and peak power that the machine should be able to produce in motor mode. For a given machine design, these values are deduced from the losses mapping model envelope described in Section 3. Both their required values are deduced from the vehicle speed and acceleration requirements.

4.3.3. Process Constraints

The only process considerations taken into account in this work are those related to the packaging requirements of the machine. The latter introduce limitations on the machine's external diameter and its total length, which considers the machine's end-windings in addition to its stack length. This then directly limits the maximum values of the external stator radius of the EM and its stack length.

4.3.4. Mechanical Constraints

During the design process, the mechanical integrity of the machine rotor under stress needs to be evaluated as well, specially at high speeds. In this work, mechanical simulations are launched at overspeed in steady state conditions for the proposed designs, as seen in Figure 4.

The overspeed value is defined as

$$\omega_{\mathrm{overspeed}} = 1.2\omega_{\mathrm{Em,max}} \tag{10}$$

The maximum value of the von Mises stress is then calculated at this speed and should be lower than the steel sheet's elastic limit, above which any deformation is irreversible [26]. Furthermore, the rotor's deformation in the radial direction should be lower than the airgap value, in order to avoid contact with the stator.

4.3.5. Thermal Constraints

Furthermore, the cooling efficiency of the machine needs to be assessed at demanding scenarios. For this study, a short-circuit at high speed is selected. Figure 5 shows the proposed thermal model of the machine. Thermal resistance values are deduced from previous test campaign results and are adjusted for each machine design while losses are adjusted using the FE model.

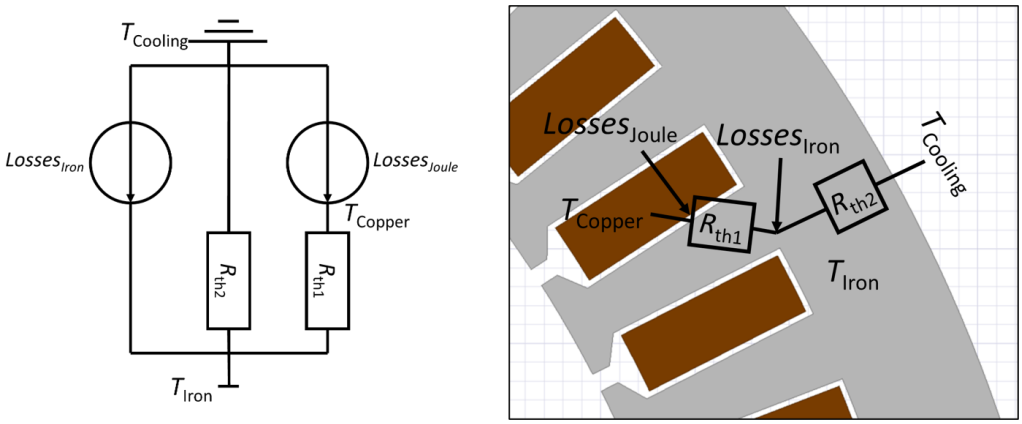

Figure 5. Thermal model of the EM. R_{th1} and R_{th2} are thermal resistances in K/W while $T_{Cooling}$, T_{Copper} and T_{Iron} are the cooling water, winding, and stator core temperatures, respectively, in °C.

The aim of the thermal study is to ensure that the winding temperature, calculated using the previous model at steady state, does not exceed the melting temperature of the conductor coating.

4.3.6. Demagnetization Constraints

The short-circuit scenario at high speed is also used to evaluate its impact on the magnet's characteristics. In this case, the stator's magnetic field is exactly opposite to the rotor's field, leading to the magnet's partial demagnetization. The used FE software allows for the possibility to reuse the demagnetized magnets. The proposed criteria for the validity of a machine design is to verify if there is no significant performance loss in this case. This means the peak torque using the demagnetized magnets needs to be equal to 95% of its previous value.

4.3.7. Torque Ripple Constraints

During the design process, the torque ripple *Ripple* of the machine needs to be monitored. It is defined as undesirable variations in the machine's output torque during its revolution and is a result of many factors such as mechanical imbalances and flux harmonics. In the case of PMSMs and the perimeter of this work, it is mainly due to the interaction between the magnetic field of the rotor magnets and the stator slots, also known as cogging torque, and can be estimated using the FE model.

The torque ripple should remain at acceptable levels and lower than a fixed threshold, especially when providing its peak torque, in order to ensure driver comfort, prevent premature wear of the drivetrain components and reduce acoustic noise.

4.3.8. Inverter Constraints

When selecting either the PWM or FW strategy, the limitations of the embedded electronics need to be considered. In fact, the PWM strategy requires at least 10 switches per electrical period compared to the FW mode which only requires a single commutation instead. This then defines $f_{PWM,max}$ and $f_{FW,max}$ which refer to the maximum commutation frequency that should be achieved by the inverter components in PWM and FW modes, respectively. Both values of $f_{PWM,max}$ and $f_{FW,max}$ are then required to be lower than the maximum switching frequency of the inverter components used in this study.

5. Proposed Approaches

5.1. Iterative Framework

The studied approaches in this paper are both based on the iterative framework, which separates both the design and control optimization blocks, as seen in Figure 6.

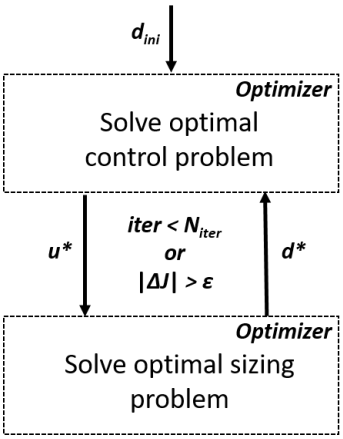

Figure 6. Iterative framework.

At first, the design variables $\boldsymbol{d}^*$ are initialized to values $\boldsymbol{d}_{\mathbf{ini}}$. The iterative framework then starts by solving the optimal control problem, expressed as

$$\boldsymbol{u}^* = \underset{\boldsymbol{u}}{\operatorname{argmin}} \quad \beta \sum_{t_0}^{t_f-\Delta t} L(\boldsymbol{d}^*, \boldsymbol{x}(t), \boldsymbol{u}(t), t)\Delta t \tag{11a}$$

$$\text{subject to} \quad \boldsymbol{x}(t+\Delta t) = \boldsymbol{f}(\boldsymbol{x}(t), \boldsymbol{u}(t), t)\Delta t + \boldsymbol{x}(t) \tag{11b}$$

$$x_1(t_0) = x_0 \tag{11c}$$

$$x_1(t_f) = x_f \tag{11d}$$

$$\boldsymbol{g}(\boldsymbol{d}^*, \boldsymbol{x}(t), \boldsymbol{u}(t), t) \leq 0 \tag{11e}$$

$$\boldsymbol{x}(t) \in [\boldsymbol{x}_{\mathbf{min}}(t), \boldsymbol{x}_{\mathbf{max}}(t)] \tag{11f}$$

$$\boldsymbol{u}^*(t) \in [\boldsymbol{u}_{\mathbf{min}}(t), \boldsymbol{u}_{\mathbf{max}}(t)] \tag{11g}$$

In this work, this problem is solved using an improved version of dynamic programming, DPAM, which has been studied and developed in [3]. The control strategy is then determined: variation of the battery's state of charge, which translates to power split between the engine and electric machine and hybrid mode selection (Regenerative braking, Full electric, Boost, or Generation), gear shifting, and starter command. The design variables are updated afterwards when solving the following optimal design problem:

$$\boldsymbol{d}^* = \underset{\boldsymbol{d}}{\operatorname{argmin}} \ \alpha Inv(\boldsymbol{d}) + \beta \sum_{t_0}^{t_f-\Delta t} L(\boldsymbol{d}, \boldsymbol{x}(t), \boldsymbol{u}^*(t), t)\Delta t \tag{12a}$$

$$\text{subject to} \quad \boldsymbol{g}(\boldsymbol{d}, \boldsymbol{x}(t), \boldsymbol{u}^*(t), t) \leq 0 \tag{12b}$$

$$\boldsymbol{k}(\boldsymbol{d}) \leq 0 \tag{12c}$$

$$\boldsymbol{d} \in [\boldsymbol{d}_{\mathbf{min}}, \boldsymbol{d}_{\mathbf{max}}] \tag{12d}$$

Figure 7 sums up the different outputs of DPAM for a proposed powertrain, over the WLTC 3-b driving cycle. For better clarity, only the last portion of the cycle (extra-high speed section) is shown. The hybrid mode selection is also shown in the same figure.

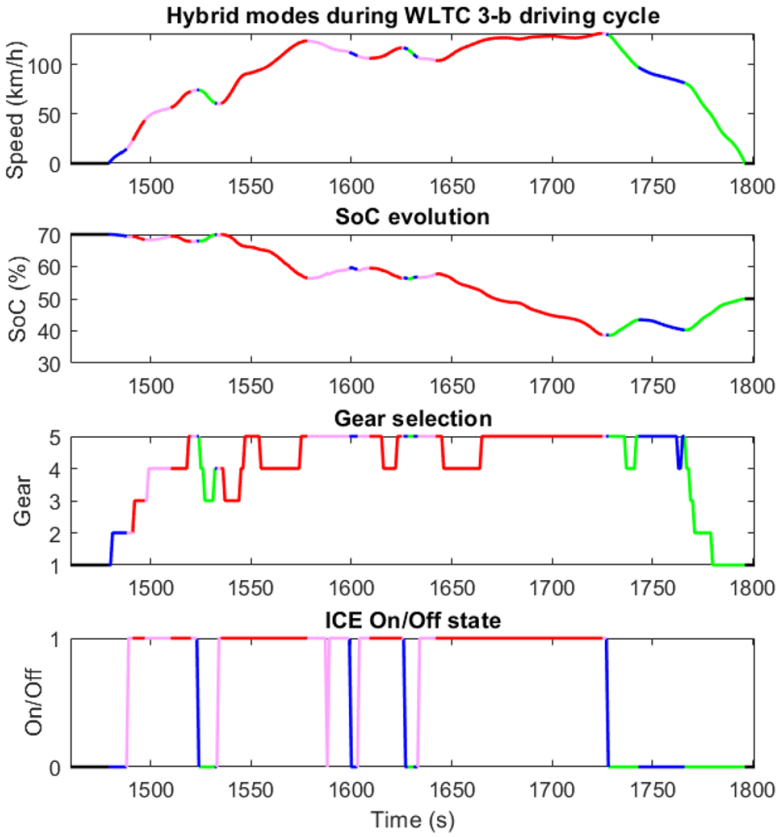

Figure 7. Optimal control results. Black: full stop, blue: Full electric mode; Red: Boost mode; Green: Regenerative Braking; Magenta: Generation mode.

This describes the first iteration of the iterative framework, which is repeated as long as cost improvements are found over a certain threshold ϵ or for a maximum number of iterations N_{iter}. It is imperative to include the controller cost when solving the design problem in order to ensure the consistency and convergence of this approach. During the design optimization process, the total energy used during the driving cycle, which is directly linked to the vehicle's fuel consumption can be expressed as

$$E_{\text{tot}} = E_{\text{u}} + E_{\text{L,EM}} + E_{\text{L,Pow}} \tag{13}$$

where E_{u} is the useful energy, and $E_{\text{L,EM}}$ and $E_{\text{L,Pow}}$ are the total energy losses of the EM and the rest of the powertrain components, respectively, during the driving cycle in J. As all of the vehicle's energy comes from the fuel tank when imposing the charge sustaining condition, the total energy used during the driving cycle can also be expressed as

$$E_{\text{tot}} = HV_{\text{gasoline}} \bar{\eta}_{\text{ICE}} \sum_{t_0}^{t_f - \Delta t} L(\boldsymbol{d}, \boldsymbol{x}(t), \boldsymbol{u}(t), t) \Delta t \tag{14}$$

where HV_{gasoline} is the heat value of gasoline in J/g and $\bar{\eta}_{\text{ICE}}$ is the mean efficiency of the engine.

When adopting the previously mentioned approach, fixing the operation points during design optimization means E_{u} is constant when varying the design parameters, as well as $E_{\text{L,Pow}}$, as the other powertrain components are not modified. This means that minimizing

E_{tot} is equivalent to minimizing $E_{L,EM}$ in this case. The design cost function to minimize becomes equivalent to

$$J(\boldsymbol{d}) = \alpha Inv(\boldsymbol{d}) + \frac{\beta}{HV_{\text{gasoline}}\bar{\eta}_{\text{ICE}}} E_{\text{L,EM}} \tag{15}$$

The Sequentially Quadratic Programming (SQP) algorithm version included in Matlab's Optimization Toolbox [27] is used to solve the aforementioned design problem. The use of this algorithm requires the design parameters to be initialized when the design optimization block is launched. Once the iterative framework converges, the optimal solution's cost is calculated using the powertrain model presented in Section 2. Figure 7 summarizes the application of the iterative framework for the hybrid vehicle application.

Two approaches are proposed afterwards using the same workflow shown in Figure 8. They differ however in how they estimate the EM losses, one of the components of the cost function, at each iteration of the SQP algorithm used for the design optimization block. Both of these variants are detailed afterwards.

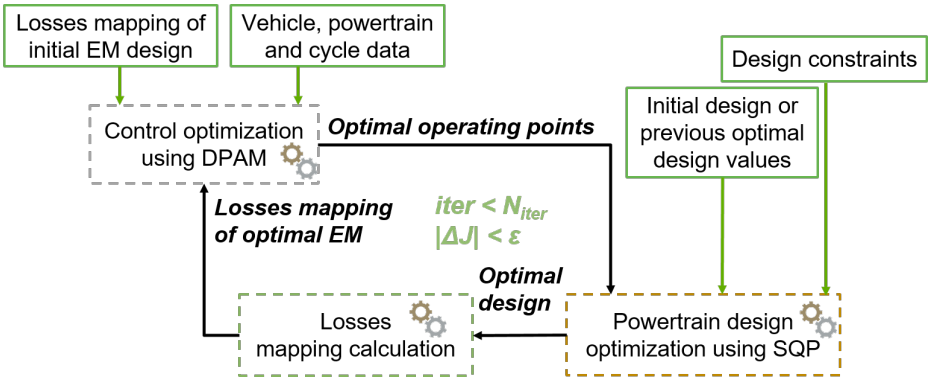

Figure 8. Application of the iterative framework for systemic design of the hybrid powertrain.

5.2. Approach *IT + MR*

The design optimization block for approach **IT + MR** is detailed in Figure 9: for every new design variables proposed by the optimization algorithm, a new losses mapping model of the machine is calculated using the process described in Section 3.5. Using the EM's optimal operating points found previously, the losses mapping of the machine allows for the direct evaluation of the machine's cycle losses.

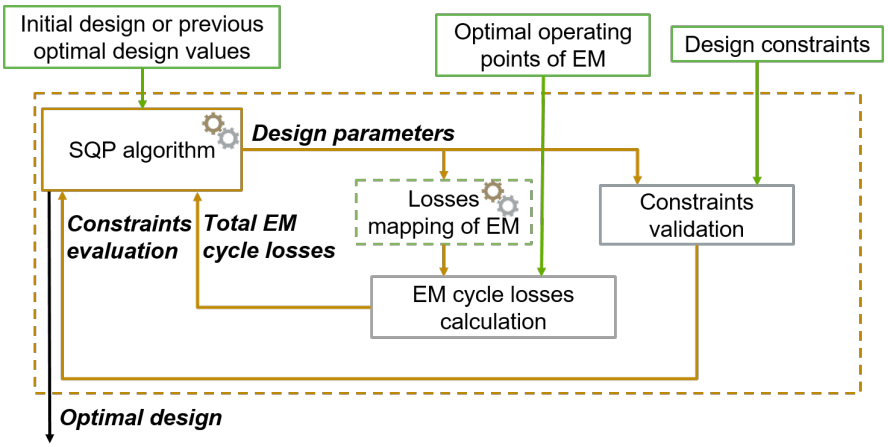

Figure 9. Design optimization block of **IT + MR** approach.

The design constraints are also evaluated at every iteration. Once an optimal design is found, the corresponding losses mapping is calculated and used for control optimization

afterwards. This optimal design also serves as initial design of the design optimization block at the next iteration of the iterative framework.

*5.3. Approach **IT + CR***

As shown in Figure 10, the second approach, **IT + CR**, uses a different method to estimate the EM cycle losses. This approach relies on cycle reduction techniques to directly estimate the machine losses using either the FE model or the circuit model of the machine, described in Sections 3.3 and 3.4, respectively. The use of cycle reduction techniques in this way is detailed afterwards. In this work, the circuit model of the machine, calculated for every new values of the design parameters, is used instead. This alternative strategy to evaluate the design cost is expected to increase the calculation speed of the model compared to the previous approach. The losses mapping of the optimal design is calculated afterwards to complete the vehicle model used for the control optimization block next. Design constraints are considered as well during the optimization process.

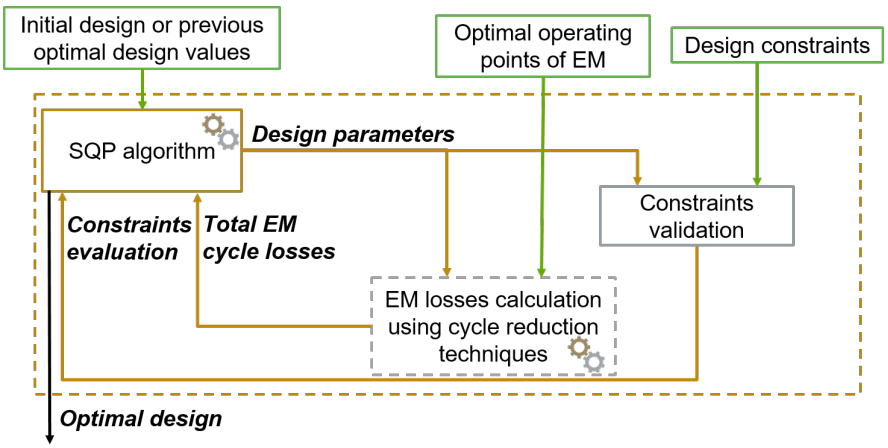

Figure 10. Design optimization block of **IT + CR** approach.

6. Cycle Reduction Techniques

Cycle reduction techniques are investigated afterwards to greatly reduce the number of the EM's operation points that are considered. This allows for faster assessment of the machine losses over the driving cycle. Four cycle reduction methods are implemented: random sampling, histogram, barycenter, and clustering methods. These methods vary first of all in the way they define the points of interest based on the thousands of operation points found for the EM during a specific driving cycle, as seen in Figure 11. These methods are packaged and provided in [28].

6.1. Studied Techniques

The random sampling method arbitrarily selects a reduced number of operation points, while the histogram and barycenter techniques divide the operation range of the machine into multiple regions before selecting their centers or barycenters, respectively. In contrast, the clustering method uses the k-means approach to form homogeneous groups of operation points called clusters, from which the barycenter is selected afterwards.

Two variants are explored to evaluate the machine losses over the driving cycle using the selected interest points. The first variant introduces an equivalency factor between the losses calculated over the interest points and the total losses over the operation points in the corresponding segment, which is expressed as

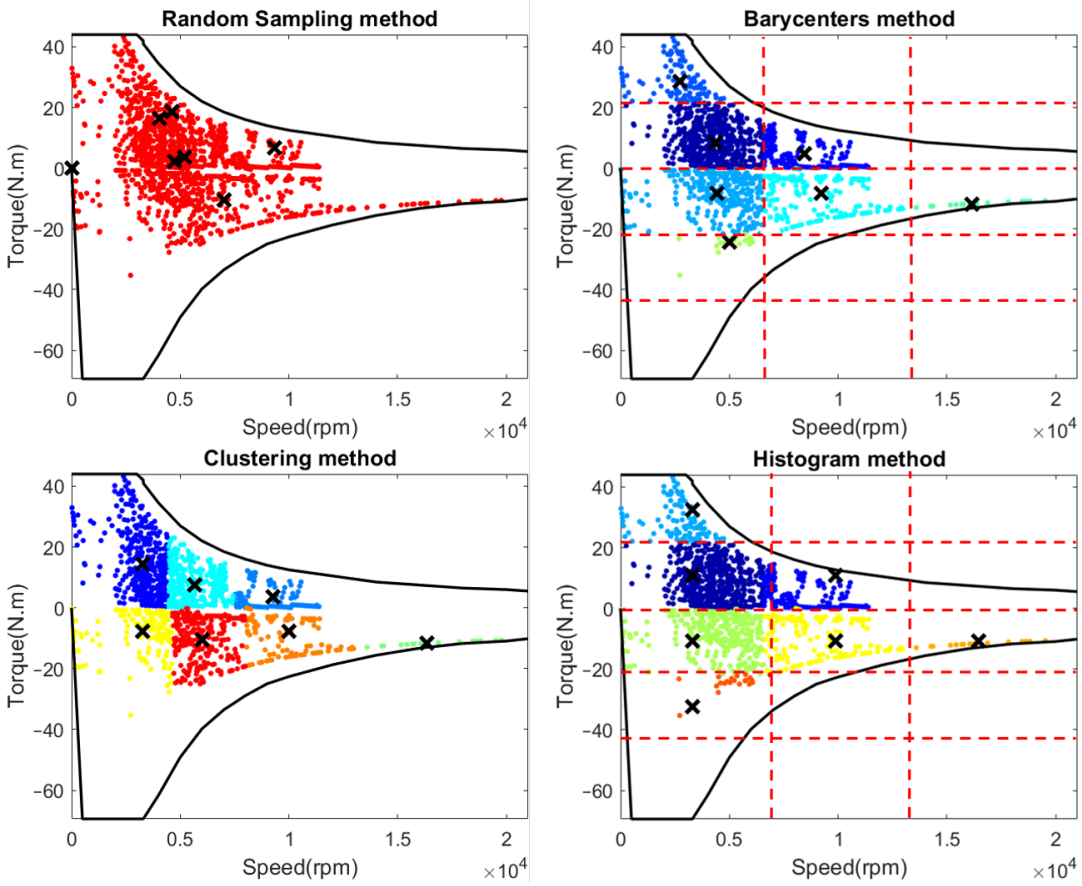

Figure 11. Application of different cycle reduction techniques.

$$k_{\mathrm{eq,i}} = \frac{\sum_{j=1}^{N_{\mathrm{pt,i}}} T_{\mathrm{EM,(i,j)}}\omega_{\mathrm{EM,(i,j)}}}{T_{\mathrm{EM,i}}\omega_{\mathrm{EM,i}}} \tag{16}$$

where $N_{\mathrm{pt,i}}$ is the number of points in group i; $T_{\mathrm{EM,(i,j)}}$ and $\omega_{\mathrm{EM,(i,j)}}$ are the torque in N.m and rotation speed values in rpm, respectively, for operation point j in segment i; and $T_{\mathrm{EM,i}}$ and $\omega_{\mathrm{EM,i}}$ are the torque in N.m and rotation speed in rpm, respectively, of interest point i.

Meanwhile, the second variant is based on employing different expressions for the different types of machine losses, as they evolve differently with respect to the torque and rotational speed values. The following expressions are given instead:

$$E_{\mathrm{Joule,cycle}} = \sum_{i=1}^{N_{\mathrm{pt}}} N_{\mathrm{pt,i}} \frac{\sum_{j=1}^{N_{\mathrm{pt,i}}} T_{\mathrm{EM,(i,j)}}{}^2}{(\sum_{j=1}^{N_{\mathrm{pt,i}}} T_{\mathrm{EM,(i,j)}})^2} Losses_{\mathrm{Joule,i}}\Delta t \tag{17}$$

$$E_{\mathrm{Iron\text{-}Hys,cycle}} = \sum_{i=1}^{N_{\mathrm{pt}}} N_{\mathrm{pt,i}} Losses_{\mathrm{Iron\text{-}Hys,i}}\Delta t \tag{18}$$

$$E_{\mathrm{Iron\text{-}EC,cycle}} = \sum_{i=1}^{N_{\mathrm{pt}}} N_{\mathrm{pt,i}} \frac{\sum_{j=1}^{N_{\mathrm{pt,i}}} \omega_{\mathrm{EM,(i,j)}}{}^2}{(\sum_{j=1}^{N_{\mathrm{pt,i}}} \omega_{\mathrm{EM,(i,j)}})^2} Losses_{\mathrm{Iron\text{-}EC,i}}\Delta t \tag{19}$$

$$E_{\mathrm{Mech,cycle}} = \sum_{i=1}^{N_{\mathrm{pt}}} N_{\mathrm{pt,i}} Losses_{\mathrm{Mech,i}}\Delta t \tag{20}$$

$$E_{\text{Inverter-Cond,cycle}} = \sum_{i=1}^{N_{\text{pt}}} N_{\text{pt,i}} \frac{\sum_{j=1}^{N_{\text{pt,i}}} T_{\text{EM,(i,j)}}{}^2}{(\sum_{j=1}^{N_{\text{pt,i}}} T_{\text{EM,(i,j)}})^2} Losses_{\text{Inverter-Cond,i}} \Delta t \tag{21}$$

$$E_{\text{Inverter-Comm,cycle}} = \sum_{i=1}^{N_{\text{pt}}} N_{\text{pt,i}} Losses_{\text{Inverter-Comm,i}} \Delta t \tag{22}$$

The machine's total losses over the cycle are then estimated as the sum of the previously calculated values for each type of losses. For the random sampling technique however, as no divisions are defined when applying this method, the following expression is proposed to estimate the cycle losses:

$$E_{\text{L,EM}} = \sum_{i=1}^{N_{\text{pt}}} k_{\text{eq,i}} Losses_{\text{pt,i}} \Delta t \tag{23}$$

with

$$k_{\text{eq,i}} = \frac{N_{\text{pt,tot}}}{N_{\text{pt}}} \tag{24}$$

where N_{pt} is the number of interest points and $N_{\text{pt,tot}}$ is the total number of operation points. $Losses_{\text{pt,i}}$ are the machine losses calculated at the interest point i in W.

6.2. Comparison and Analysis

The studied techniques with both alternatives for loss calculation are applied afterwards to estimate the losses of an electric machine over the WLTC (Worldwide harmonized Light vehicles Test Cycle) 3-b driving cycle, while only selecting 10 points of interest. Table 1 summarizes the results of the comparison, where deviations between the output values for each type of machine losses found when using cycle reduction methods and the real total cycle losses are presented in relative values.

Table 1. Deviation between the proposed cycle reduction techniques over 10 interest points and real cycle losses.

	Joule (%)	Iron (Hys) (%)	Iron (EC) (%)	Mech (%)	Comm (%)	Cond (%)	Total Losses (%)
Random sampling	20.72	5.61	23.13	11.73	11.63	15.81	**17.93**
Histogram (var. 1)	13.23	12.02	5.46	8.44	3.53	8.00	**7.61**
Histogram (var. 2)	13.23	9.14	2.11	4.92	3.53	8.00	**5.06**
Barycenters (var. 1)	17.07	0.64	7.77	3.94	10.63	13.60	**9.56**
Barycenters (var. 2)	17.07	2.08	0.28	0.27	10.63	13.60	**6.02**
Clustering (var. 1)	14.42	0.04	1.45	1.19	4.89	9.28	**5.29**
Clustering (var. 2)	14.43	1.04	0.45	0.00	4.92	9.30	**4.34**

It can be observed that the second variant for each technique leads to better results. Furthermore, when considering the total machine losses, it can be deduced that the clustering method is the most accurate among the studied methods. This can be enhanced by considering more interest points. However, the required calculation time when implementing the selected method will also increase proportionally.

6.3. Mirroring Technique

We propose a novel technique to improve the precision of the studied methods without increasing the number of interest points. This method, named Mirroring and shown in Figure 12, assumes that close loss values are found for two machine operation points of opposite electromagnetic torque values defined by (ω_{EM}, T_{El}) and (ω_{EM}, $-T_{\text{El}}$). The technique then "mirrors" the operation points in motor mode into the generator operation range of the EM, before applying any of the previously mentioned cycle reduction methods.

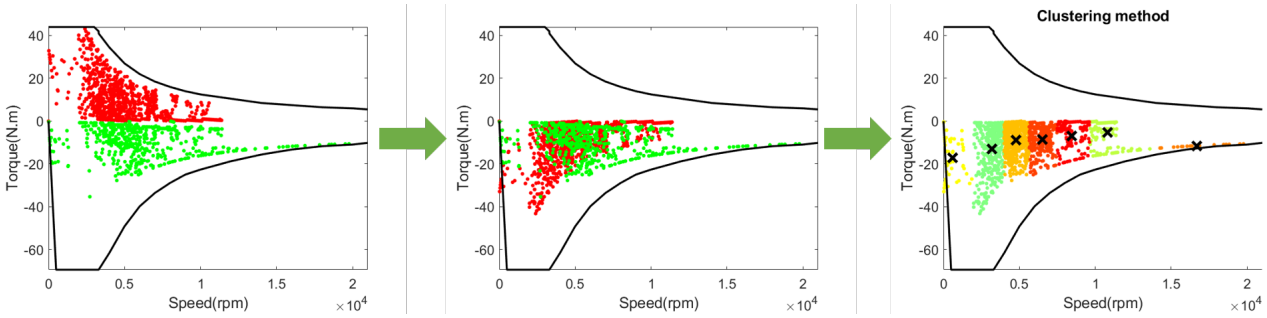

Figure 12. Mirroring technique principle applied using the clustering method.

This approach allows for a much more accurate division of one of the machine modes without modifying the total number of interest points selected. Table 2 presents the results when applying this method using the second variant of the clustering technique for the same application described before.

Table 2. Comparison between the proposed cycle reduction techniques. Deviations are calculated in relative value compared to cycle loss values.

	Joule	Iron (Hysteresis)	Iron (EC)	Mechanical	Commutation	Conduction	Total Losses
Original (%)	14.43	1.04	0.45	0.00	4.92	9.30	4.34
With Mirroring (%)	3.90	0.34	0.43	0.00	0.66	1.44	0.86

It can be seen that the accuracy of the technique has greatly improved in this case, with a general deviation in total losses of less than 1%. This method is then selected for use with approach **IT + CR**.

7. Application and Results

7.1. Optimization Application

The characteristics as well as the features of the different powertrain components for the HEV case study are presented in Table 3.

Table 3. Studied vehicle characteristics.

Component	Notation	Value
Vehicle	Vehicle's mass	1470 kg
	First rolling resistance coefficient	4.57×10^{-3}
	Second rolling resistance coefficient	1.79×10^{-4} s/m
	Aerodynamic coefficient	0.6044 m^2
	Wheel radius	0.2032 m
Battery	Battery capacity	54,000 A.s
	Maximum battery output current	310
	Initial state of charge	50%
	Final state of charge	50%
	Open circuit voltage	45.31 V
	Internal resistance	0.0118 Ω
Auxiliaries	Auxiliary consumption	0 W
Machine	Air gap	0.5 mm
	Cooling water temperature	75 °C
Transmission	Transmission ratios	{14.80;7.98;4.76;3.26;2.45}
Engine	Engine inertia	0.259 $kg.m^2$
	Engine maximum speed	6250 rpm
	Engine idle speed	750 rpm
	Peak power	81 kW

The problem presented in Section 4 is then solved, with the vehicle's fuel consumption evaluated over the WLTC 3-b cycle and Δt set to 1 s. This cycle is selected as it has been designed to be more representative of the real and modern driving conditions compared to previous homologation procedure, becoming the reference cycle for measuring CO_2 emissions [29]. This measurement will take place in laboratory conditions on a flat and dry road.

The various design constraints enumerated in Section 4 are considered afterwards. Based on a given set of machine and project requirements, key values necessary to validate the machine design are deduced. These parameters are listed in Table 4.

The large number of design variables present in the original optimization problem however should be reevaluated, as this will lead to longer optimizations as well as convergence difficulties afterwards. Different options should be assessed to reduce the number of variables considered and allow for an optimal machine design to be found in reasonable delays.

Table 4. Required values for the definition of EM design constraints.

Parameter	Value
Required value for the EM's peak output power	25 kW
Required value for the EM's peak output torque	70 N.m
Maximum EM speed	21,000 rpm
Maximum value for the EM's external diameter	161 mm
Maximum value for the EM's total length	119 mm
Metal sheet's elastic limit	365 MPa
Melting temperature of the conductor coating	250 °C
Maximum value for the torque ripple	15%
Inverter component maximum switching frequency	10 kHz

7.2. Screening Study

The presence of 32 design variables has prompted the launch of screening experiments, in a bid to reduce the number of decision variables during optimization. This study is one of the main stages of the design of experiments (DoE), a widely used tool in engineering that maximizes learning about a system or a process while using minimum resources [30,31].

Screening designs are used to scout the search space when little is known about the mathematical models used for the optimization application. It is possible afterwards to deduce the impact of each studied parameter, but interactions between the latter are hard to interpret. For this study, a reduced number of experiments are selected using Sobol's Quasirandom Sequence to achieve uniform distribution over the search space [32]. An initial pool sample of 346 designs, over 10 times the total number of design variables, is chosen to achieve acceptable accuracy. The cost function is calculated using DPAM, while the various constraints adopt the models described previously. The impact of each factor is evaluated using Pearson's correlation coefficient [33].

As constrained optimizations are conducted afterwards, this selection should be based on the impact of these factors on all of the outputs displayed above and not only the cost function by itself. Figure 13 shows the global impact of each design parameter. The global impact is a weighted sum of effects where the impact on fuel consumption is given a weight of 3, while all the other outputs discussed earlier are attributed a uniform weight of 1.

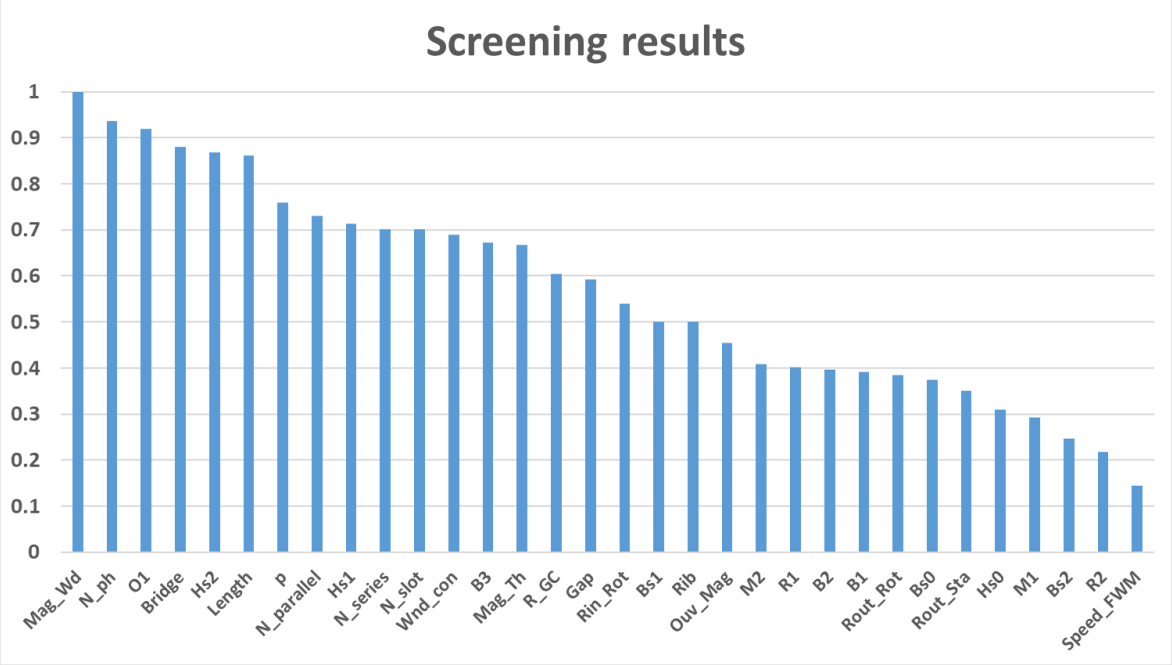

Figure 13. Normalized global impact of the design parameters deduced from conducted screening experiments.

7.3. Optimization Results

The solutions found by each variant of the iterative approach are compared afterwards to an existing design referred to as REF. The machine in question satisfies the various requirements of the design application and was optimized for maximum efficiency at a single operation point: peak torque at 1000 rpm. It must be noted that the fuel consumption and total cost values are recalculated using the EM losses mapping model.

A first comparison is conducted based on the optimization of 4 continuous parameters. These are selected following the conclusions of the screening study (d_1: Mag_{Wd}, d_2: *O1*, d_3: *Bridge*, d_4: *Hs2*). The other design parameters are fixed and are equal to those of the reference design, which also serves to initialize the chosen optimization variables when using the different approaches.

The selection of the continuous parameters over the discrete parameters has been made to simplify the search process. Their recommended values, determined based on the previous screening process, are found to correspond to the initial design's values.

The average distance between the optimal parameters and their reference $dist_{\mathrm{Avg}}$ and the maximum distance to reference $dist_{\mathrm{Max}}$ are evaluated as well and calculated using the following expressions:

$$dist_{\mathrm{Avg}} = \frac{1}{N}\sum_{i=1}^{N}\frac{|d_{\mathrm{i,ref}} - d_{\mathrm{i}}{}^{*}|}{d_{\mathrm{i,max}} - d_{\mathrm{i,min}}} \tag{25}$$

$$dist_{\mathrm{Max}} = \max_{i}\frac{|d_{\mathrm{i,ref}} - d_{\mathrm{i}}{}^{*}|}{d_{\mathrm{i,max}} - d_{\mathrm{i,min}}} \tag{26}$$

where N is the number of optimization variables while $d_{\mathrm{i,min}}$ and $d_{\mathrm{i,max}}$ refer, respectively, to the lower and upper bounds for optimization variable d_{i}. $d_{\mathrm{i,ref}}$ and d_{i}* correspond, respectively, to its reference and optimal values. Table 5 compiles the optimization results. The difference in total cost *J*, EM cost *Inv*, and CO_2 emissions between the optimal designs and the reference machine in € is estimated, as well as the number of cost function evaluations and total calculation time in s.

Table 5. Comparison of systemic design approaches based on 4 optimization variables.

Approach	IT + MR	IT + CR
$dist_{Avg}$	0.0906	0.1225
$dist_{Max}$	0.2747	0.3333
Total cost reduction	377 €	253 €
EM cost reduction	87 €	60 €
CO_2 emissions reduction	3.05 gCO_2/km	2.03 gCO_2/km
Fuel consumption reduction	0.13 l/100 km	0.09 1/100 km
Peak power	25.02 kW	26.37 kW
Peak torque	79.19 N.m	70.00 N.m
Maximum speed	21,000 rpm	21,000 rpm
Torque ripple	8.07%	0.89%
Peak copper temperature	152 °C	146 °C
Total length	115 mm	115 mm
External diameter	161 mm	161 mm
Number of cost function evaluations	252	331
Calculation time	125,019 s	128,536 s

The solutions provided by each approach satisfy the imposed constraints. High values of both $dist_{Avg}$ and $dist_{Max}$ demonstrate the ability of both approaches to search for the optimal solution outside the immediate vicinity of the initial design. In terms of total cost reduction, the best solution is the one proposed by **IT + MR**. Approach **IT + CR** on the other hand, which is based on cycle reduction techniques, should consider additional clusters in order to find similar solutions to those found by approach **IT + MR**. Calculation time can be improved for example by relaxing the tolerance of the iterative loop, set at 0.1 € for this application and launching more FE simulation in parallel.

A second comparison is launched afterwards for 10 optimization variables, identified based on the findings in Figure 13 as well: machine design parameters Mag_{Wd}, *O1*, *Bridge*, *Hs2*, *Length*, *Hs1*, *Bs1*, *B3*, Mag_{Th}, and gear connection ratio R_{GC}. Table 6 summarizes the comparison results.

Table 6. Comparison of systemic design approaches based on 10 optimization variables.

Approach	IT + MR	IT + CR
$dist_{Avg}$	0.0952	0.0550
$dist_{Max}$	0.5861	0.3784
Total cost reduction	661 €	424 €
EM cost reduction	85 €	71 €
CO_2 emissions reduction	6.06 gCO_2/km	3.72 gCO_2/km
Fuel consumption reduction	0.26 l/100 km	0.16 1/100 km
Peak power	25.12 kW	25.82 kW
Peak torque	70.00 N.m	70.00 N.m
Maximum speed	21,000 rpm	21,000 rpm
Torque ripple	14.27%	7.19%
Peak copper temperature	135 °C	184 °C
Total length	109 mm	103 mm
External diameter	155 mm	161 mm
Number of cost function evaluations	681	459
Calculation time	336,087 s	177,841 s

As expected, adding more optimization variables leads to better cost reductions when using the various systemic design approaches, while significantly increasing calculation times. This justifies once more the importance of limiting the number of decision variables to obtain optimization results in reasonable delays. The use of the iterative framework makes approaches **IT + MR** and **IT + CR** sensitive to the selected design initialization [5]. Increasing the number of initial guesses will improve the quality of their solutions. Furthermore, computation times for both approaches can be easily divided by 5 folds when launching even more FE simulations in parallel.

8. Conclusions

In this work, the electric machine of a parallel hybrid powertrain is optimized. An extended hybrid vehicle model is presented, which considers the impact of the battery's SoC variation, gear shifting, and engine stop/restart with an iso-granularity representation for all the powertrain components.

In order to quickly and accurately estimate the EM's performance, a losses mapping model, based on parallel finite element simulations and Park's PMSM representation, is used. This model can be recalculated rapidly for new machine parameters and leads to deviations of less than 2% when confronted to prototype tests.

Different command and design constraints are enumerated, which consider the powertrain limitations and the machine requirements. Thus, the complete hybrid powertrain optimization problem is defined. Once a case study for the optimization application is selected, a screening analysis is launched to identify the most vital factors.

Two different systemic design strategies based on the iterative framework are proposed. The first approach, **IT + MR**, is based on the use of the parametric losses mapping model at every iteration of the design algorithm while the second approach relies on precise cycle reduction techniques to estimate machine losses. The second approach, **IT + CR**, can enable the direct use of high precision models without penalizing the calculation time.

Important cost reduction is then achieved in reasonable computation times, which translates in part into improved fuel efficiency. This also cements the importance of systemic design in exploiting the hybrid powertrain to its fullest and leading to much better fuel economy as compared to focusing on the optimization of a single component, which is the case of the reference machine used for initialization.

IT + MR is more precise and leads to better solutions while **IT + CR** is faster. The cost gains of both approaches can be improved by increasing the number of initial guesses. Their calculation time can also be reduced through more parallelization of FE calculations.

These approaches can be easily applied for the systemic design of the other powertrain components, which requires the development of adequate parametric models to reflect the impact of the design parameters over their performance. Application over other powertrain architectures is possible as well once an efficient control strategy is selected and the necessary powertrain model adjustments are made. Comparison with other systemic design strategies such as the ones based on the bi-level and simultaneous frameworks also needs to be undertaken over the same application for better assessment.

Author Contributions: Conceptualization, A.K.; methodology, A.K.; software, A.K.; validation, A.K., S.B., M.A., R.V., and M.O.; formal analysis, A.K.; investigation, A.K.; writing—original draft preparation, A.K.; writing—review and editing, A.K., S.B., M.A., R.V., and M.O.; visualization, A.K.; supervision, S.B., M.A., R.V., and M.O. All authors have read and agreed to the published version of the manuscript.

Funding: This research received no external funding.

Conflicts of Interest: The authors declare no conflicts of interest.

Abbreviations

The following abbreviations are used in this manuscript:

DPAM	Dynamic programming with adaptive meshing
EM	Electric machine
FE	Finite Element
FW	Full wave
HEV	Hybrid electric vehicle
ICE	Internal combustion engine
PMSM	Permanent Magnet Synchronous Machine
PWM	Pulse-width modulation
SQP	Sequential Quadratic Programming
WLTC	Worldwide harmonized Light vehicles Test Cycles

Appendix A

After selecting an existing machine and identifying the machine parameters $\boldsymbol{d}$, the parametric FE model's accuracy is assessed based on the experimental results of said machine and the 3D FE calculations of the same machine.

The different results are summarized in the following tables, with deviations determined between the bench test values and calculations of the parametric FE model. BT refers to the bench test results, while CAD and PM are correspondingly the 3D FE model and parametric FE model results and the compared quantities are the mainly used outputs in the optimization study.

The no load results are compiled in Table A1. They mainly focus on the root mean square (rms) value of the back EMF voltage (EMF) and its first harmonic (EMF-h1) at different magnet temperatures and rotational speeds.

Table A1. Comparison results for no load scenarios.

	BT (Vrms)	CAD (Vrms)	PM (Vrms)	Deviation (%)
EMf at 25 °C/1000 rpm	9.72	9.71	9.77	−0.51
EMF-h1 at 25 °C/1000 rpm	9.70	9.76	9.68	−0.20
EMf at 80 °C/1000 rpm	9.38	9.38	9.40	−0.21
EMF-h1 at 80 °C/1000 rpm	9.33	9.33	9.33	0.00
EMf at 110 °C/1000 rpm	9.21	9.18	9.08	1.41
EMF-h1 at 100 °C/1000 rpm	9.16	9.13	9.00	1.75

Table A2 on the other hand shows the obtained rms value of the steady state short-circuit current for the three cases at high speed (6000 rpm).

Table A2. Comparison results on a short-circuit scenario.

BT (Arms)	CAD (Arms)	PM (Arms)	Deviation (%)
220.7	227.1	224.1	−1.50

Finally, Table A3 compares the average mechanical torque values obtained at multiple operation points of the machine, in both generator and motor modes. The current phase is calculated so as to minimize the losses in the machine.

The different results presented in the three tables show maximum deviations, of around 2%, for the measured quantities.

Table A3. Comparison results for on-load scenarios.

	BT (N.m)	CAD (N.m)	PM (N.m)	Deviation (%)
Motor mode at 355 Arms/0 rpm	95.0	94.9	95.0	0.00
Motor mode at 234 Arms/1000 rpm	70.0	68.8	68.8	1.65
Motor mode at 195 Arms/2000 rpm	60.0	59.0	58.9	1.83
Motor mode at 217 Arms/3000 rpm	60.0	60.6	61.1	−1.80
Motor mode at 164 Arms/5000 rpm	40.0	40.2	40.0	−0.01
Generator mode at 131 Arms/6000 rpm	−30.0	−30.1	−30.0	0.12

References

1. Wu, H.; Alberts, G.; Hopper, J.; Walton, B. *New Market. New Entrants. New Challenges. Battery Electric Vehicles*; Deloitte LLP: London, UK, 2019.
2. Morgan, J.P. Driving into 2025: The Future of Electric Vehicles. 2018. Available online: https://www.jpmorgan.com/global/research/electric-vehicles (accessed on 1 October 2020).
3. Kaloun, A.; Brisset, S.; Ogier, M.; Reynouard, M.; Ahmed, M.; Mipo, J.C. Comparison and analysis of control strategies for hybrid electric vehicles. In Proceedings of the 2019 IEEE Vehicle Power and Propulsion Conference (VPPC), Hanoi, Vietnam, 14–17 October 2019.
4. Fathy, H.K.; Reyer, J.A.; Papalambros, P.Y.; Ulsoy, A.G. On the Coupling between the Plant and Controller Optimization Problems. In Proceedings of the American Control Conference, Arlington, VA, USA, 25–27 June 2001.
5. Fathy, H.K.; Papalambros, P.Y.; Ulsoy, A.G. On combined Plant and Control optimization. In Proceedings of the 8th Cairo University International Conference on Mechanical Design and Production, Cairo University, Cairo, Egypt, 8–10 January 2012.
6. Sundström, O. Optimal Control and Design of Hybrid-Electric Vehicles. Ph.D. Thesis, ETH Zurich, Zurich, Switzerland, 2009,
7. Yaich, M.; Hachicha, M.R.; Ghariani, M. Modeling and simulation of electric and hybrid vehicles for recreational vehicle. In Proceedings of the 16th IEEE International Conference on Sciences and Techniques of Automatic Control and Computer Engineering (STA), Monastir, Tunisia, 21–23 December 2015; pp. 181–187.
8. Fellini, R.; Michelena, N.; Papalambros, P.; Sasena, M. Optimal design of automotive hybrid powertrain systems. In Proceedings of the 1st International Symposium on Environmentally Conscious Design and Inverse Manufacturing, EcoDesign 1999, Tokyo, Japan, 1–3 February 1999; pp. 400–405.
9. Wenzhong, G.; Porandla, S.K.; Gao, W.; Porandla, S.K. Design optimization of a parallel hybrid electric powertrain. In Proceedings of the 2005 IEEE Vehicle Power and Propulsion Conference (VPPC), Chicago, IL, USA, 7 September 2005; Volume 2005, pp. 530–535. [CrossRef]
10. Donateo, T.; Serrao, L.; Rizzoni, G. A two-step optimisation method for the preliminary design of a hybrid electric vehicle. *Int. J. Electr. Hybrid Veh.* **2008**, *1*, 142–165. [CrossRef]
11. Williamson, S.S.; Khaligh, A.; Oh, S.C.; Emadi, A. Impact of energy storage device selection on the overall drive Train efficiency and performance of heavy-duty hybrid vehicles. In Proceedings of the 2005 IEEE Vehicle Power and Propulsion Conference VPPC, Chicago, IL, USA, 7 September 2005; pp. 381–390. [CrossRef]
12. Nüesch, T.; Ott, T.; Ebbesen, S.; Guzzella, L.; Nuesch, T.; Ott, T.; Ebbesen, S.; Guzzella, L. Cost and fuel-optimal selection of HEV topologies using particle swarm optimization and dynamic programming. In Proceedings of the 2012 American Control Conference (ACC), Montreal, QC, Canada, 27–29 June 2012; pp. 1302–1307.
13. Hofman, T.; Ebbesen, S.; Guzzella, L. Topology optimization for hybrid electric vehicles with automated transmissions. *IEEE Trans. Veh. Technol.* **2012**, *61*, 2442–2451. [CrossRef]
14. Caillard, P. Conception par Optimisation d'une Chaine de Traction Électrique et de son Contrôle par Modélisation Multi-physique. Ph.D. Thesis, Ecole Centrale de Lille, Villeneuve-d'Ascq, France, 2016.
15. Reinbold, V. Méthodologie de Dimensionnement d'un Moteur éLectrique pour vÉhicules Hybrides: Optimisation Conjointe des Composants et de la Gestion D'énergie. Ph.D. Thesis, Université de Grenoble, Grenoble, France, 2015.
16. Desai, C.; Williamson, S.S. Optimal design of a parallel Hybrid Electric Vehicle using multi-objective genetic algorithms. *IEEE Veh. Power Propuls. Conf.* **2009**, 871–876. [CrossRef]
17. Fang, L.; Qin, S.; Xu, G.; Li, T.; Zhu, K. Simultaneous optimization for hybrid electric vehicle parameters based on multi-objective genetic algorithms. *Energies* **2011**, *4*, 532–544. [CrossRef]
18. Bayrak, A.E.; Kang, N.; Papalambros, P.Y. Decomposition-Based Design Optimization of Hybrid Electric Powertrain Architectures: Simultaneous Configuration and Sizing Design. *J. Mech. Des. Trans. ASME* **2016**, *138*, 1–9. [CrossRef]
19. Michelena, N.; Park, H.; Papalambros, P. Convergence properties of analytical target cascading. In Proceedings of the 9th AIAA/ISSMO Symposium on Multidisciplinary Analysis and Optimization, Atlanta, Georgia, 4–6 September 2002; Volume 41.
20. Guzzella, L.; Sciarretta, A. *Vehicle Propulsion Systems: Introduction to Modeling and Optimization*; Springer: Berlin/Heidelberg, Germany, 2013.

21. Fratila, M. Contribution à la Prise en Compte des Pertes fer dans la Modélisation des Machines Électriques par Élements Finis. Ph.D. Thesis, Université Lille, Lille, France, 2012.
22. Park, R.H. Two-Reaction Theory of Synchronous Machines: Generalized Method of Analysis-Part I. *Trans. Am. Inst. Electr. Eng.* **1929**, *48*, 716–727. [CrossRef]
23. Silvas, E.; Bergshoeff, E.; Hofman, T.; Steinbuch, M. Comparison of bi-level optimization frameworks for sizing and control of a hybrid electric vehicle. In Proceedings of the 2014 IEEE Vehicle Power and Propulsion Conference (VPPC), Coimbra, Portugal, 27–30 October 2014.
24. Ebbesen, S.; Elbert, P.; Guzzella, L. Engine Downsizing and Electric Hybridization Under Consideration of Cost and Drivability. *Oil Gas Sci. Technol.—Rev. d'IFP Energies Nouv.* **2013**, *68*, 109–116. [CrossRef]
25. Pourabdollah, M.; Murgovski, N.; Grauers, A.; Egardt, B. Optimal sizing of a parallel PHEV powertrain. *IEEE Trans. Veh. Technol.* **2013**, *62*, 2469–2480. [CrossRef]
26. Jones, R.M. *Deformation Theory of Plasticity*; Bull Ridge Publishing: Blacksburg, VA, USA, 2009.
27. MathWorks. Constrained Nonlinear Optimization Algorithms. Available online: https://fr.mathworks.com/help/optim/ug/constrained-nonlinear-optimization-algorithms.html (accessed on 1 October 2020).
28. Kaloun, A. Cycle Reduction Toolbox for Matlab. Available online: https://www.mathworks.com/matlabcentral/fileexchange/81403-cycle-reduction-toolbox-for-matlab (accessed on 1 October 2020).
29. Mohr, D.; Müller, N.; Krieg, A.; Gao, P.; Kaas, H.W.; Krieger, A.; Hensley, R. The road to 2020 and beyond: What's driving the global automotive industry? *Adv. Ind.* **2013**.
30. Altekar, M.; Homon, C.A.; Kashem, M.A.; Mason, S.W.; Nelson, R.M.; Patnaude, L.A.; Yingling, J.; Taylor, P.B. Assay optimization: A statistical design of experiments approach. *Clin. Lab. Med.* **2007**, *27*, 139–154. [CrossRef] [PubMed]
31. Ghanem, R.; Higdon, D.; Owhadi, H. *Handbook of Uncertainty Quantification*; Springer: Berlin/Heidelberg, Germany, 2017.
32. Bratley, P.; Fox, B.L. Algorithm 659 Implementing Sobol's Quasirandom Sequence Generator. *ACM Trans. Math. Softw.* **1988**, *14*, 88–100. [CrossRef]
33. Kent State University. SPSS Tutorials: Pearson Correlation. Available online: https://libguides.library.kent.edu/SPSS/PearsonCorr (accessed on 1 October 2020).